Medical Engineering and Physics 71 (2019) 17–29

Contents lists available at ScienceDirect

Medical Engineering and Physics

journal homepage: www.elsevier.com/locate/medengphy

Personalized 3D-printed endoprostheses for limb sparing in dogs: Modeling and *in vitro* testing

Anatolie Timercan[a], Vladimir Brailovski[a,*], Yvan Petit[a], Bertrand Lussier[b], Bernard Séguin[c]

[a] Department of Mechanical Engineering, École de technologie supérieure, 1100 Notre-Dame West, Montreal, Quebec H3C1K3, Canada
[b] Faculty of Veterinary Medicine, Université de Montréal, 3200 Sicotte, Saint-Hyacinthe, Quebec J2S2M2, Canada
[c] Colorado State University Flint Animal Cancer Center, 300 W Drake, Fort Collins, Colorado 80525, USA

ARTICLE INFO

Article history:
Received 30 July 2018
Revised 21 June 2019
Accepted 4 July 2019

Keywords:
Personalized implant
Additive manufacturing
Numerical validation
Limb sparing
Biomechanical testing

ABSTRACT

Osteosarcoma is the most common type of bone cancer in dogs, treatable by amputation or limb-sparing surgery. For the latter, commercially available plate – endoprosthesis assemblies require contouring, to be adapted to the patient's bone geometry, and lead to sub-optimal results. The use of additively-manufactured personalized endoprostheses and cutting guides for distal radius limb-sparing surgery in dogs presents a promising alternative.

Specialized software is used for the bone structure reconstruction from the patient's CT scans and for the design of endoprostheses and cutting guides. The prostheses are manufactured from a titanium alloy using a laser powder bed fusion system, while the cutting guides are manufactured from an ABS plastic using a fused deposition modeling system. A finite element model of an instrumented limb was developed and validated using experimental testing of a cadaveric limb implanted with a personalized endoprosthesis.

Personalized endoprostheses and cutting guides can reduce limb sparing surgery time by 25–50% and may reduce the risk of implant failure. The numerical model was validated using the kinematics and force-displacement diagrams of the implant-limb construct. The model indicated that a modulus of elasticity of an implant material ranging from 25 to 50 GPa would improve the stress distribution within the implant. The results of the current study will allow optimization of the design of the personal implants in both veterinary and human patients.

1. Introduction

Over the past thirty years, additive manufacturing technologies, also known as 3D printing, have evolved significantly. They offer the possibility of creating functional parts with complex geometries, which are difficult to reproduce using conventional manufacturing technologies [1]. New materials, such as high strength polymers and various metallic alloys, are being developed and adapted for additive manufacturing, which increases the number of possible applications. 3D printing offers agility and tool-free production, which makes this technology perfectly suited for the manufacture of patient-specific (personalized) implants [2,3]. This study focuses on the design, 3D printing, modeling, and in vitro testing of patient-specific endoprostheses for limb-sparing surgery in dogs affected by osteosarcoma of the distal radius.

1.1. Osteosarcoma

Osteosarcoma (OS) is the most common form of bone cancer that affects dogs. Each year, over 10,000 dogs are afflicted with OS in the United States [4]. This type of cancer mainly involves large breed dogs, such as Rottweilers, German Shepherds, Great Danes, and Dobermans [5,6]. Studies have shown that the predominant factor in the development of osteosarcoma is the weight and size of the dog, rather than its breed [4]. Generally, OS occurs at the appendicular skeleton (75%), affecting the long bones (radius, ulna, humerus, femur, tibia), the most common site being the distal radius [5,7], as illustrated in Fig. 1.

Common care practices include amputation and limb-sparing surgery with adjuvant chemotherapy. Amputation of the limb affected by osteosarcoma is the most commonly used technique. With this relatively simple operation, the tumor is completely removed, and the risks of complications and infection are minimized.

Abbreviations: OS, Osteosarcoma; LPBF, Laser Powder Bed Fusion.

* Corresponding author.
E-mail addresses: anatolie.timercan.1@ens.etsmtl.ca (A. Timercan), vladimir.brailovski@etsmtl.ca (V. Brailovski), yvan.petit@etsmtl.ca (Y. Petit), bertrand.lussier@umontreal.ca (B. Lussier), bernard.seguin@colostate.edu (B. Séguin).

https://doi.org/10.1016/j.medengphy.2019.07.005
1350-4533/

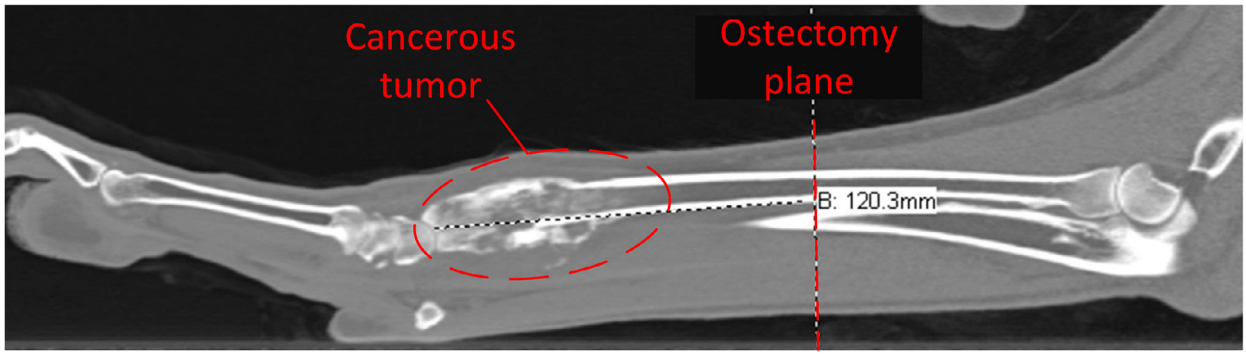

Fig. 1. CT-scan pilot view of a forelimb afflicted by OS of the distal radius (Flint Animal Cancer Center, Colorado State University).

However, the risks of metastasis remain high, and the average life expectancy ranges from 18 to 20 weeks [8,9]. A combination of adjuvant chemotherapy with amputation has been shown to increase the average life expectancy to 43 to 45 weeks [10,11]. Nonetheless, as osteosarcoma affects large and giant breeds dogs which are also afflicted by degenerative joint disease, it often renders these patients poor candidates for amputation. Moreover, some dog owners are opposed to amputation as a treatment since this intervention can affect the quality of life of their pets [12].

The alternative to amputation is limb-sparing surgery, which consists of ostectomy of a part of the affected bone and resection of certain carpal tendons followed by the installation of a metallic construct to bridge the remaining bone structures. Such a treatment often involves arthrodesis of the adjacent joint, and since the appendicular OS occurs most commonly at the distal radius or proximal humerus, the limb-sparing surgery results in the immobilization of the carpus or shoulder, respectively. The shoulder being a crucial joint allowing correct limb function in quadruped mammals, its immobilization significantly compromises the function of the limb [13,14]. Conversely, because arthrodesis of the carpus is much less detrimental, limb-sparing surgery in dogs for the distal radius is performed more commonly [8,15]. Although life expectancy after limb-sparing surgery remains similar to that following amputation (40 to 41 weeks) [15,16], the benefit of preserving the patient's limb function makes this treatment worthwhile.

There are multiple variants for limb sparing of the distal radius. Firstly, the distal aspect of the radius where the tumor is arising from is resected. Then, a bone graft or metal endoprosthesis is placed in the defect resulting from the ostectomy. Bone grafts can take the form of cortical bone allografts [17] or autografts via ulna transposition, intraoperative radius pasteurization or irradiation [7,18–20]. Finally, a metal plate is screwed into the bone graft or metal endoprosthesis, into the third metacarpal, and into the residual radius. The main limitation of using the radial autograft is that it requires intra-operative irradiation or pasteurization, which results in extended surgery time. For allografts, the necessity of a canine bone bank is costly and time consuming. The use of a plate-endoprosthesis all-metal construct (Fig. 2) constitutes, therefore, a promising alternative.

1.2. Commercial limb-sparing implants

There are only a few types of bone plates and endoprostheses commercially available for limb-sparing surgeries in dogs. These implants are generally made of 316 L stainless steel, with some companies offering titanium variants. For example, only two plate lengths and two endoprosthesis lengths are available at Veterinary Orthopedic Implants (VOI, USA) to accommodate a plethora of tumor and dog sizes. To offer a better stability to a limb-sparing construct, the bone plates are generally provided with conical threads in the screw holes to receive self-locking head screws [21].

The disadvantage of commercial bone plates is the need to adapt them to the remaining bone structures by performing intra-operative contouring, which has limited degrees of freedom. In addition, since commercial endoprostheses are only available in a very limited number of sizes, the cut lengths must also be adapted. These tasks lengthen the surgery and increase the number of intra-/extra-corporeal manipulations, thus potentially increasing the risks of infection. As a result of such a suboptimal treatment, there is also the risk of implant/bone failure and loosening/breaking of the screws (36–40%) [15,22].

1.3. Personalized implants design and manufacturing

Some recent works [23–25] proposed the design of personalized implants using bone structures reconstructed from the CT scan of the patient, and the production of these implants using metal additive manufacturing technologies. The advantage of such an approach is to provide an adapted implant for each patient. This approach would decrease surgical time, thus potentially decreasing postoperative infections, would be individualized, thus improving the implant fit in the implantation site, and, finally, the design of every implant could be optimized, thus making it more resistant to failure. Since this approach is relatively new, only few examples are reported in the literature. For example, Bray, Kersley [26] designed and manufactured personalized limb-sparing implants using laser powder bed fusion technology. In that case, a solid plate covered the metacarpals and the remaining part of the radius was connected to a porous structure replacing the removed radius. This approach aimed to offer the possibility of bone ingrowth, for better implant fixation, and reduced stiffness, for improving the load sharing at the implantation site. Note that no modeling of the implant-limb behavior was carried out in this case, which limits the results obtained to the specific implant geometry.

1.4. Testing and modeling of limb-sparing implants

To assess the mechanical behavior of bone plate-endoprosthesis constructs, one must rely on biomechanical testing of instrumented cadaveric limbs. To this end, Horn [27] carried out biomechanical testing of limbs implanted with personalized limb-sparing implants; the testing setup was inspired by Liptak, Ehrhart [14] and Pooya, Seguin [28]. The personalized implants were similar in design to those in Bray, Kersley [26], and were manufactured using electron beam powder bed fusion of Ti-6Al-4 V powder. The instrumented limbs were placed in a standard materials testing system and then compressed to simulate the weight of the dog. The input loading on the implant represented a complex combination of compression and bending, and the output data provided the

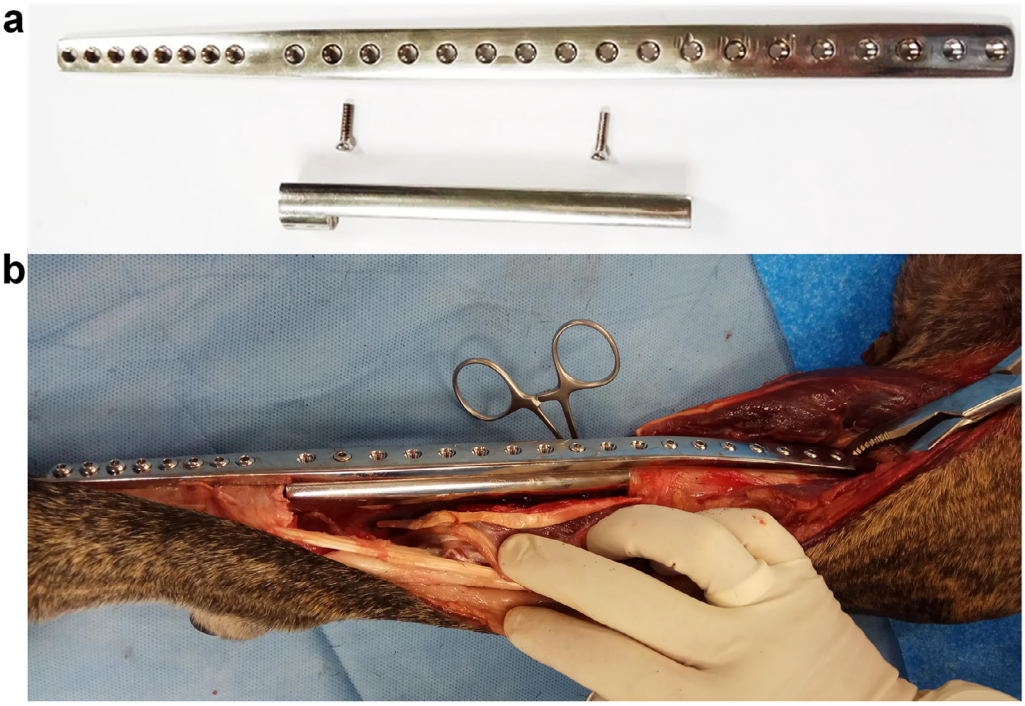

Fig. 2. (a) Commercial bone plate and endoprosthesis (Veterinary Orthopedic Implants [VOI], USA), (b) limb-sparing surgery at the distal radius using a commercial plate and endoprosthesis (Université de Montréal, Faculty of Veterinary Medicine).

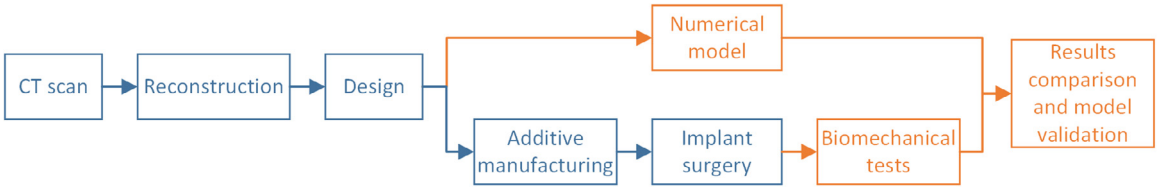

Fig. 3. Methodology employed in this study; technological workflow in blue; model validation in orange.

stiffness of the implant-limb construct under these loading conditions. Note that in this case, as in the preceding work of Bray, Kersley [26], no modeling of the implant-limb behavior was carried out.

On the other hand, Shetye [29] built a numerical model of the dog limb using the CT-scan data and validated this model by carrying out biomechanical testing of an intact cadaveric limb. Following validation, the model was used to develop a new type of modular endoprosthesis. Note, however, that these prostheses were neither manufactured nor tested.

To compensate for some limitations of the previous studies, this study is intended to offer an integrated approach for the design, manufacturing, numerical modeling and biomechanical testing of personalized endoprostheses for dogs. The novel endoprostheses, coupled with personalized cutting guides, are intended to reduce the duration of surgery and the risks of post-surgical complications. The numerical model of the implant-bone construct is destined to serve for prosthesis design optimization.

2. Materials and methods

The personalized endoprosthesis in this work is composed of a bone plate which reproduces the bone curvature and a spacer, which replaces the excised affected radius. The cutting guide uses the ulnar styloid process and the lateral ulna for positioning, and incorporates a cutting slot that affixes over the radius [30].

Fig. 3 depicts the methodological approach of this study, which is divided into two parts: the design and manufacturing workflow, extending from the data acquisition (CT scan) to surgery, and the numerical model workflow, including the model development and its experimental validation.

2.1. Technological workflow from data acquisition to surgery

2.1.1. Reconstruction

A CT scan with a 1 mm slice thickness is performed at the veterinary clinic on both front limbs of the ailing dog. The limbs are positioned with extension of the antebrachiocarpal joint with a normal standing angle determined for each individual dog. The veterinary surgeon identifies the tumor on the CT scan and marks the optimal cutting distance from the antebrachiocarpal joint, taking into consideration a 5 cm margin of safety beyond the border of the tumor. The DICOM images are transferred through cloud storage to the engineering team. The images are processed with Mimics Research19 (Materialise, Leuven, Belgium), and the reconstructed bone structures are used for the implant and cutting guide designs (Fig. 4.1–4). A segmentation procedure is finally carried out to separate the radius, ulna and carpal/metacarpal bones on the affected limb and the healthy radius, on the contralateral limb (Fig. 4.5). The bone models are smoothed and exported in STL format into a CAD environment (Fig. 4.6).

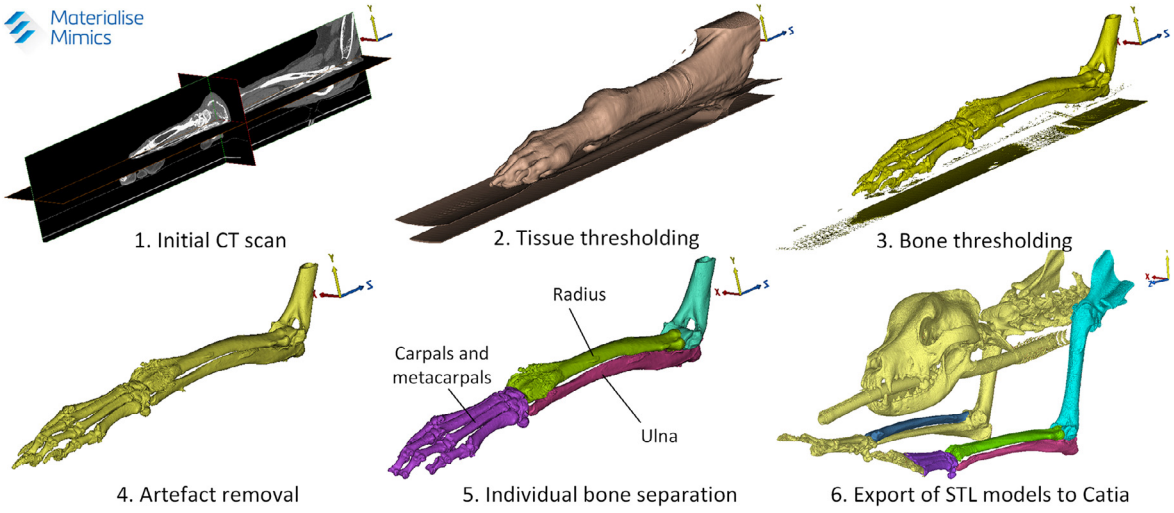

Fig. 4. Bone structure reconstruction stages.

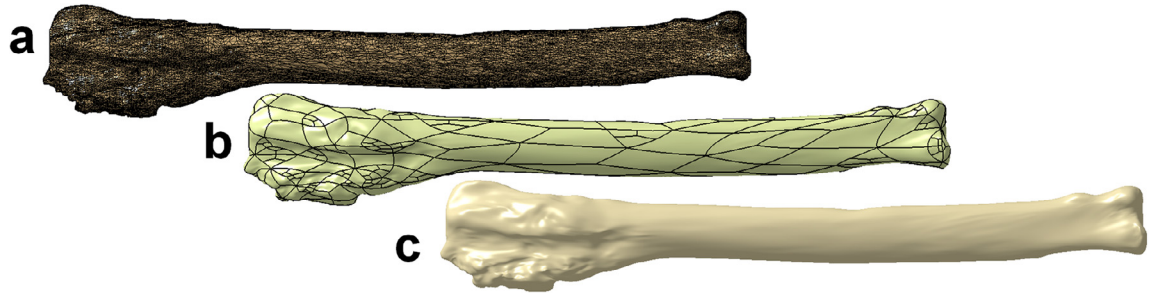

Fig. 5. Bone model conversion stages (radius): (a) STL representation, (b) surface model, (c) solid model.

2.1.2. Computer-aided design

Fig. 5 illustrates the bone model conversion from STL to solid, using Catia V5R21 software (Dassault Systèmes, Vélizy-Villacoublay, France).

The contralateral (healthy) radius which is of similar size and proportion is mirrored and superposed on the affected radius (Fig. 6b). Next, the osteotomy plane is created at the prescribed distance perpendicular to the long axis of the bone (Fig. 6c). The affected part of the radius is virtually removed and replaced by its healthy counterpart (Fig. 6d). A contoured plate, featuring conical self-locking threaded holes, is created to accept commercially-offered screws (Fig. 6e-f). Afterward, the contoured plate, the healthy radius section and an intramedullary stem, corresponding to 70% of the intramedullary canal diameter are joined via additive Boolean operations. Then, subtractive Boolean operations are carried out with the objective of ensuring perfect surface contact between the endoprosthesis and the bones: the carpal/metacarpal bones and the salvaged part of the affected radius are removed from the plate. Finally, the implant thickness is verified and thin areas are reinforced (Fig. 6g).

A parametric cutting guide template is then placed on the radius and adjusted to comply with the bone geometry. It features a cutting slot that coincides with the previously created osteotomy plane, ensuring correct alignment between the cut and the endoprosthesis (Fig. 7). To create matching surfaces, Boolean operations of removal are performed on the guide using the ulna and radius solid models.

Before the manufacturing stage, the endoprosthesis and guide designs are validated with the veterinary surgeon and then converted into STL file format.

2.1.3. Manufacturing of endoprosthesis and cutting guide

The endoprosthesis is manufactured using a Ti-6Al-4 V alloy powder (Ti64) and a laser powder bed fusion (LPBF) EOSINT M280 400 W Ytterbium fiber laser system (EOS GmbH, Munich, Germany) (Fig. 8.3). This alloy has the advantage of being corrosion- and mechanically-resistant, low-stiffness and lightweight material (yield stress of 1000 MPa, Young's modulus of 110 GPa, and density of 4.41 g/cm^3). Multiple studies in recent years have discussed the biocompatibility of additively-manufactured Ti64 medical parts, concluding that this material is suitable for use in load-bearing implants [31–36].

Given that the LPBF process fuses powder locally, significant thermal stresses are induced in the part due to rapid temperature changes and significant temperature gradients. To prevent resulting thermal distortions and stabilize the parts during manufacturing, supports that bind the parts to the manufacturing plate are generated beforehand, using Magics 17 software (Materialise, Leuven, Belgium). A combination of fully dense and hatch supports is used to ensure firm attachment of the part to the build plate. During manufacturing, as illustrated in Fig. 8.1, the endoprosthesis is oriented horizontally, thus reducing the build time and the amount of powder feedstock required, both being proportional to build height. The disadvantage of this orientation is that it involves a large amount of support structures, which need to be removed after manufacturing.

Once the supports are generated, model slicing and laser path programming are performed using the PSW 3.6 software (EOS GmbH, Munich, Germany) (Fig. 8.2). Fabrication parameters were set to the 'EOS Ti64 Performance Parameters Set', which uses 30 µm-thick layers. After manufacturing, the solid parts and the

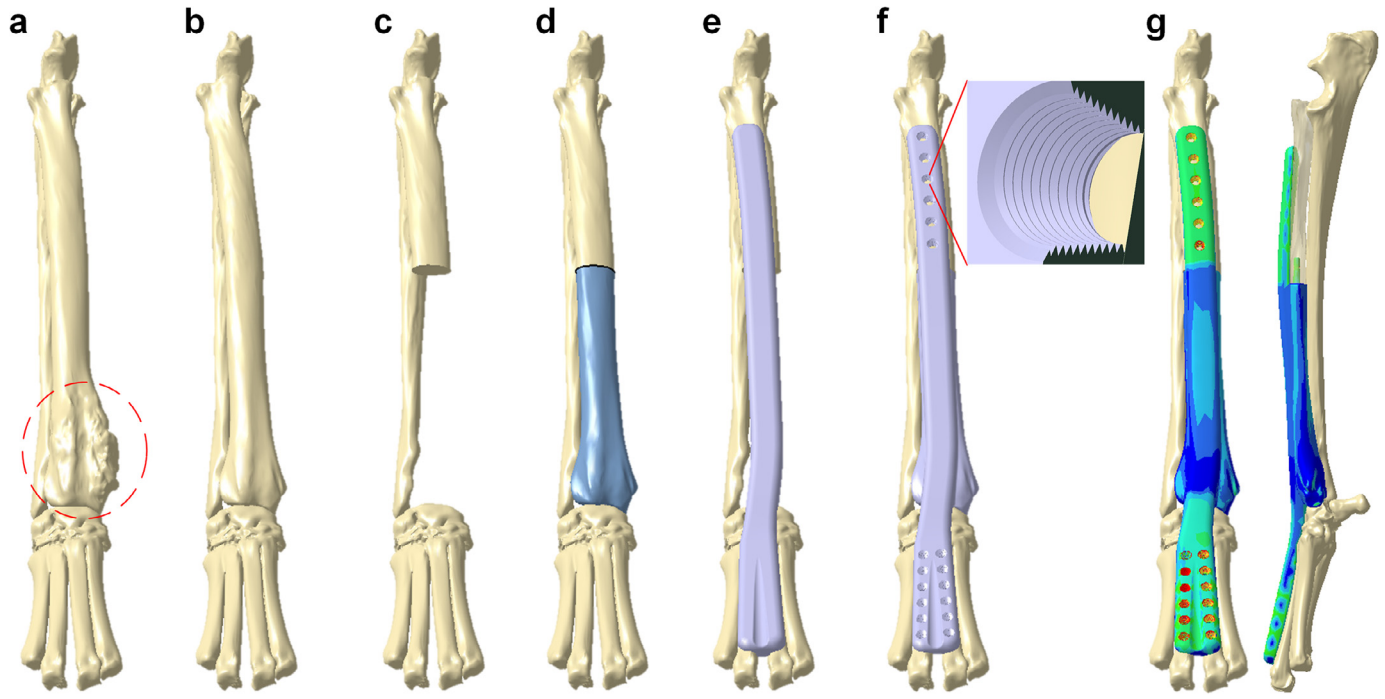

Fig. 6. Prosthesis design stages (a) solid bone models of the affected limb, (b) mirror and positioning of the healthy contralateral radius, (c) resection of the affected part of the radius using cutting plane, (d) replacement with the healthy radius, (e) design of the contoured plate, (f) placement of holes and consolidation with healthy radius section (g) thickness verification and adjustment.

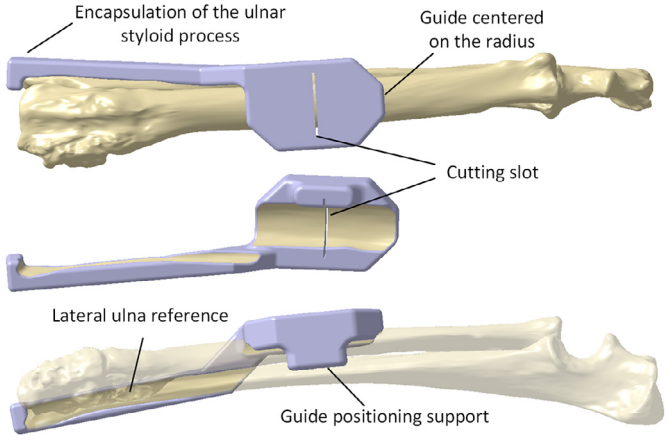

Fig. 7. Cutting guide design.

build plate are cleaned of loose powder (Fig. 8.4). Residual stresses are released by performing an EOS-recommended 4-hour heat treatment at 800 °C in an inert gas (argon) atmosphere (Fig. 8.5). During heat treatment, the build plate is placed in a protective gas box of an N41/H furnace (Nabertherm GmbH, Lilienthal, Germany), and ultra-high purity argon (5.0) is pumped into the box at the following rates: 15 L/min during the treatment and 25 L/min, during preflushing and cooling.

The separation of the parts from the manufacturing plate is performed by cutting the supports, using a Baxter horizontal band saw. This is followed by finishing and polishing steps using files, tungsten carbide burrs, sanding and a MicroPeen 250 microblasting piece of equipment (IEPCO AG. Switzerland) with 0.5 mm steel shot media. Surfaces in contact with the skin are fine-polished, while those in contact with bones and muscles are simply microblasted (Fig. 8.6). The self-locking threads in the conical holes are rectified using custom-manufactured hand taps. The finished endoprosthesis is cleaned in an ultrasonic bath with a cleaning solvent.

The cutting guide is fabricated from ABS plastic using a Fortus 250mc fused deposition modeling system (Stratasys Ltd., Minneapolis, USA) (Fig. 9.2). The part interior is designed using fully dense rendering, and the horizontal build orientation is chosen to minimize build height and the quantity of support material (Fig. 9.1). 'Smart' supports are generated using Insight 11.9 software (Stratasys Inc., Minnesota, USA). After printing, the part is placed in a WaterWorks solution ultrasonic bath for dissolution of supports.

The endoprosthesis and cutting guide kit are now ready to be shipped to the veterinary clinic, where sterilization must be performed before surgery.

2.2. Numerical model and experimental testing

2.2.1. Biomechanical testing

The finite element model and the experimental testing of this study were inspired by the biomechanical test setups proposed by Liptak, Ehrhart [14], Horn [27], Pooya, Seguin [28], Shetye [29]. In all these studies, cadaveric dog limbs were instrumented using different limb-sparing techniques; the extremities of the humerus and phalanges were embedded in custom fixtures, and the elbows, positioned at angles varying between 125°–135°, which is representative of normal limb positioning. In this study, these setups were modified to allow free longitudinal travel of the metacarpals, with the objective of avoiding application of a flexural moment on the load cell (Fig. 10).

The forelimb of a 70 kg Great Dane afflicted by osteosarcoma of the distal radius, which had been euthanized at the request of his owners, was salvaged for this study and preserved at −25 °C after being covered with tissues soaked with saline solution. The limb was CT-scanned and a personalized endoprosthesis was designed and manufactured, following the previously described procedure. Self-tap cortical screws were purchased from Veterinary

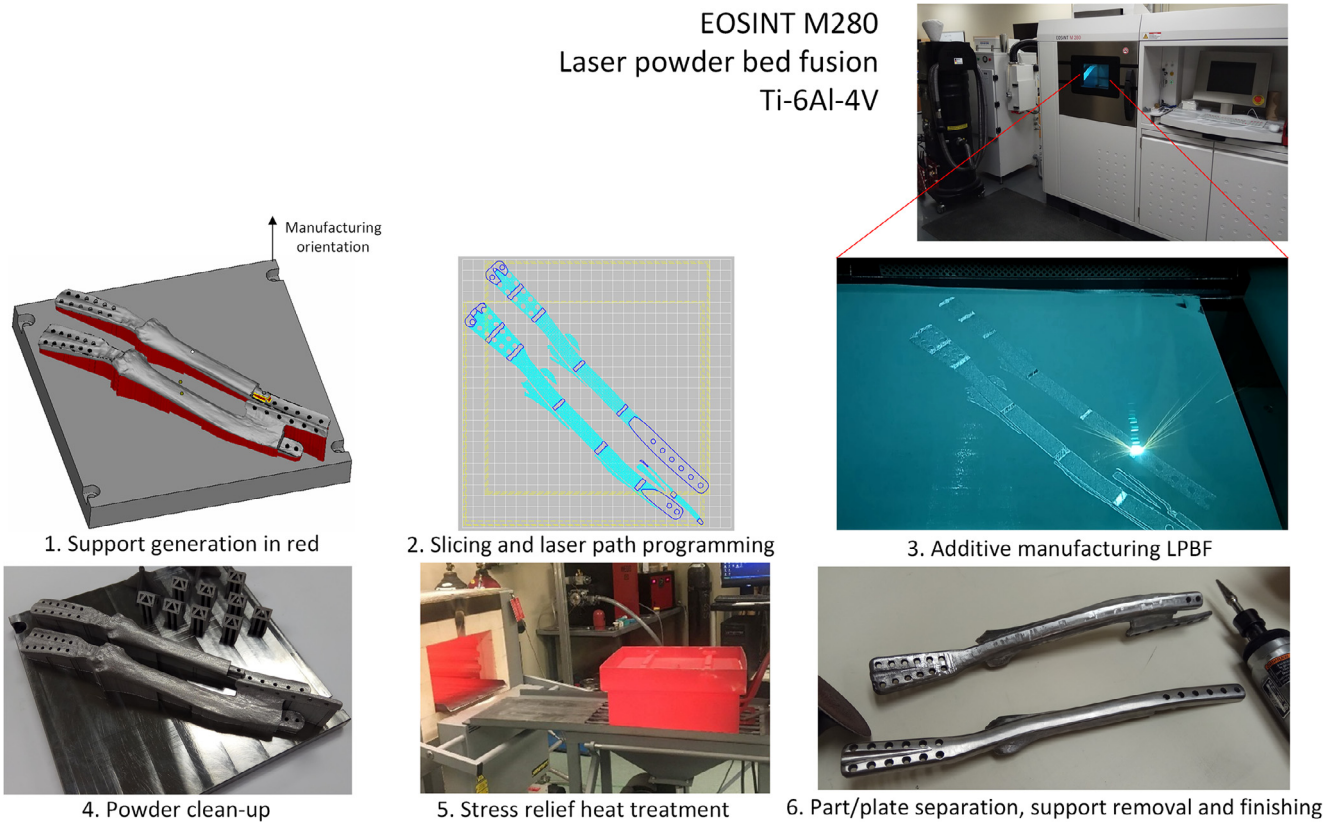

Fig. 8. Prosthesis manufacturing stages.

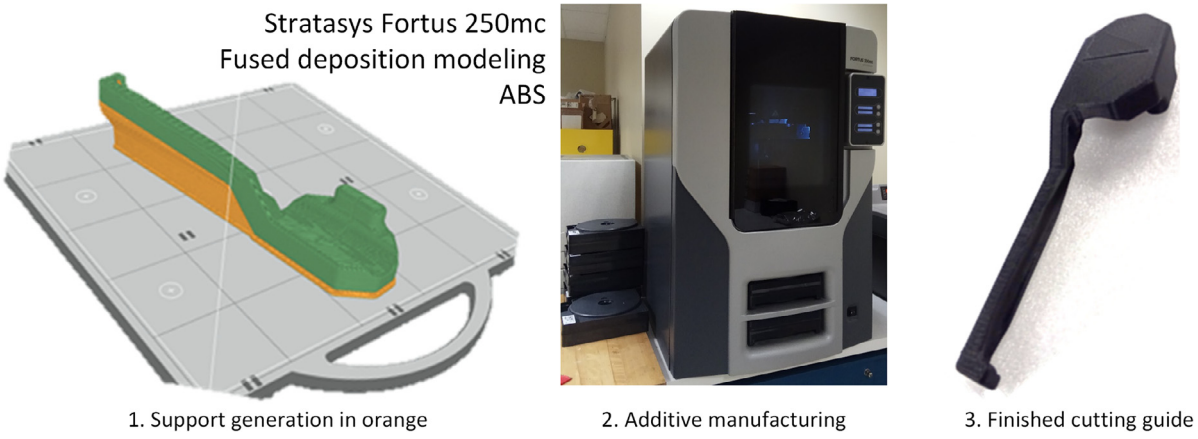

Fig. 9. Manufacturing steps of the personalized cutting guide.

Orthopedic Implants (VOI, USA), for a total of twelve 2.7 mm and six 3.5 mm screws for use in the distal and proximal portions of the personalized endoprosthesis, respectively.

2.2.2. Non-linear numerical analysis

The reconstructed solid bone models and personalized endoprosthesis with screws were imported as STP files in Ansys Workbench 18.2 (ANSYS, Canonsburg, PA, USA). Only cortical bones were modeled, and screw threads were not designed. Resin embeddings were created around the humerus and metacarpals. The material properties displayed in Table 1 were applied to the various components and the boundary conditions were imposed as illustrated in Fig. 11a. All the materials were assumed to have isotropic bilinear behavior.

The size and complexity of the CT scanned bone geometry proved to be too costly in terms of computational power requirements. To facilitate model solving, bones were represented as hollow tubes with outside diameters and wall thicknesses corresponding to the average values of the cortical bone structure. The personalized endoprosthesis was modeled as a straight plate extending from the salvaged part of the radius to the metacarpals. The plate covered two metacarpals and was combined with a cylindrical part representing the removed part of the radius. The symmetry was exploited to reduce the mesh size and the large deflections option was activated. The medial collateral, lateral collateral and interosseous ligaments of the elbow joint were defined as spring elements on the surfaces corresponding to the attachment points determined from the CT scan. The ligament stiffness was taken as 70 N/mm [39,40]. The contact conditions between

Table 1
Numerical model material properties (E is the Young's modulus; ν is the Poisson's coefficient; S_y is the yield stress; UTS is the ultimate tensile strength; A is the elongation to failure).

Material	Properties				
	E (GPa)	ν	S_y (MPa)	UTS (MPa)	A (%)
Bone [37,38]	15	0.3	40	110	4
Ti-6Al-4 V (EOS datasheet)	110	0.33	945	1055	13
Urethane resin (Axson datasheet)	2.7	0.35	30	50	3

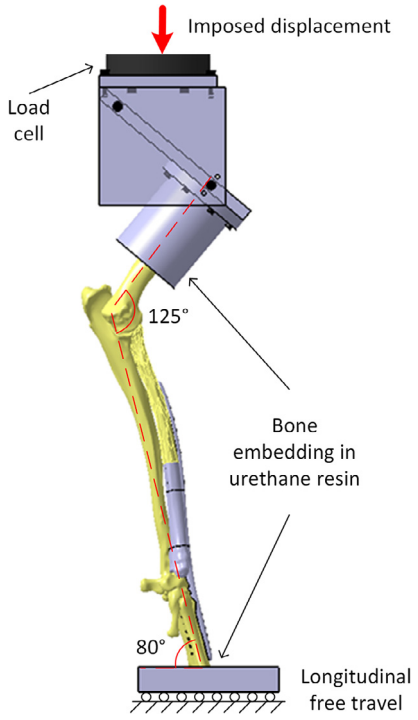

Fig. 10. Testing configuration used in the present study.

the model components were defined as shown in Fig. 11b. The Advanced Lagrangian contact formulation with a 0.5 stiffness coefficient was used to facilitate model solving, and resulted in negligible contact penetration. A convergence study was conducted to obtain a mesh with 37,144 tetrahedral elements and 75,655 nodes.

2.2.3. Experimental testing

The cadaveric limb of the Great Dane was instrumented using the proposed personalized limb-sparing technique at the Université de Montréal's Faculty of Veterinary Medicine. In the proximal part of the construct, six 3.5 mm cortical screws were used (Fig. 12), while twelve 2.7 mm cortical screws were used in its distal part to affix the endoprosthesis to the third and fourth metacarpals. All screws were applied in neutralization mode.

Biomechanical testing was conducted at the Research Center of the Sacré-Cœur de Montréal Hospital. To this end, muscles were stripped away from the humerus and metacarpals, with care taken to leave ligaments intact. Custom fixtures were used to embed the limb extremities in F100 polyurethane resin (Axson Technologies, France), as can be seen in Fig. 13. A 0.9% saline solution was used to keep the specimen moistened throughout dissection and testing.

Fig. 14 illustrates limb installation in an MTS 858 Bionix II with a 15 kN uniaxial load cell (MTS System Inc., Eden Prairie, MN, USA). The elbow was positioned at an angle of about 125°, and the metacarpal fixture was installed on a uniaxial translation table. Markers were placed on the endoprostheses and fixtures, and tracked with an ARAMIS 5 M non-contact optical measurement

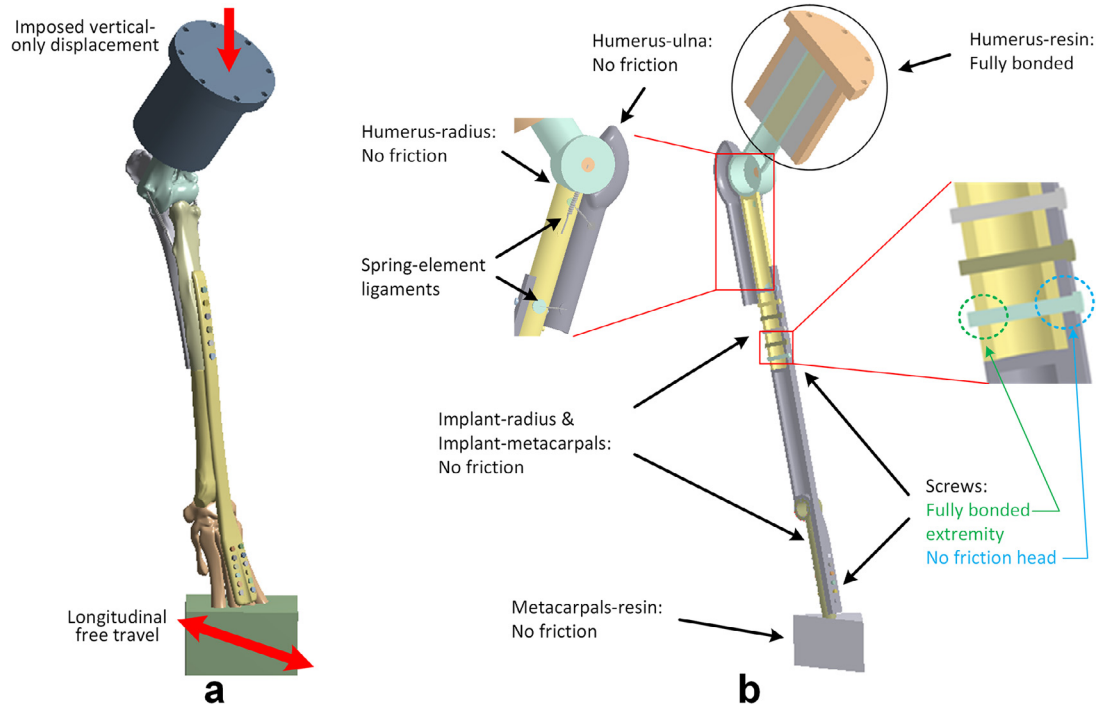

Fig. 11. (a) CT-issued geometry finite element model, (b) simplified finite element model.

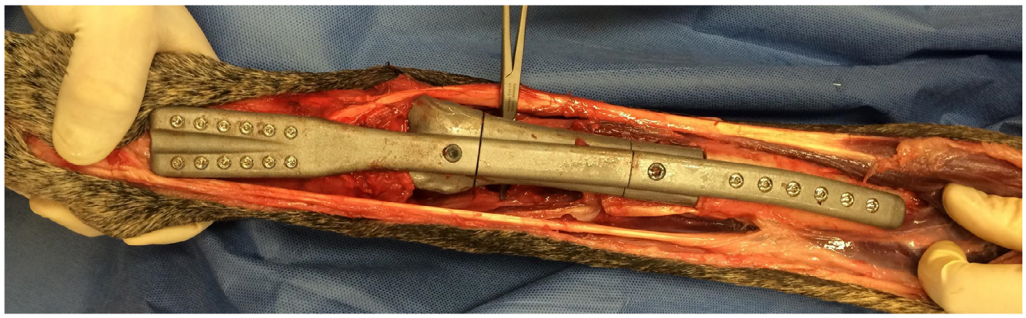

Fig. 12. Cadaveric limb instrumentation with the personalized endoprosthesis.

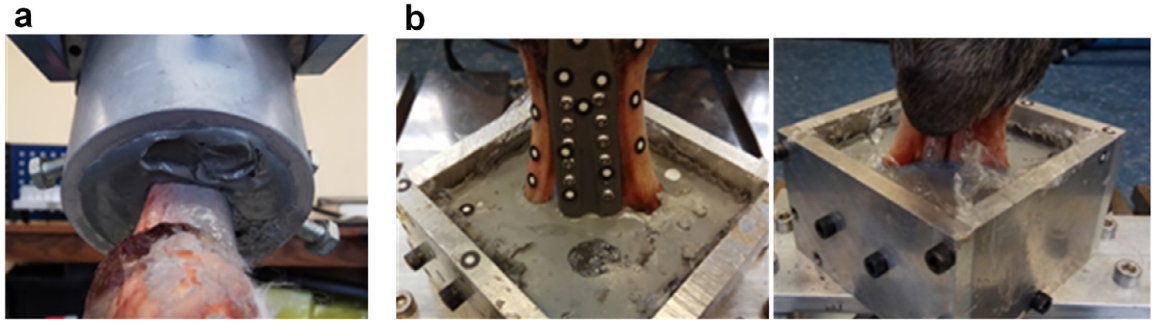

Fig. 13. Bone extremities embedded in polyurethane resin: (a) humerus, (b) metacarpals.

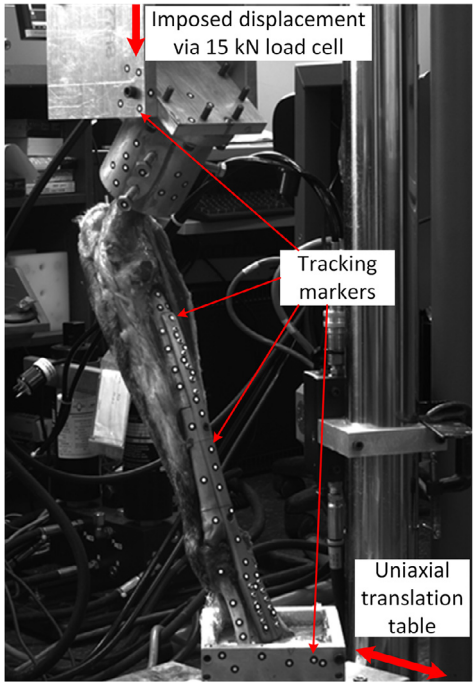

Fig. 14. Test setup for the personalized endoprosthesis.

system (GOM mbH, Braunschweig, Germany). The instrumented limb was then tested in compression with a crosshead speed of 0.5 mm/s. Forces and crosshead displacements were measured using a load cell and an LVDT of the MTS, respectively.

2.3. Model validation

Three-stage model validation was carried out by comparing the numerically modeled and the experimentally measured data. To this end, implant-limb kinematics was evaluated using numerical probes created at positions corresponding to the tracking markers placed on the endoprosthesis and fixtures (Fig. 15). Next, the images captured by the Aramis system were treated using ProAnalyst (Xcitex Inc, USA) software to calculate marker displacements (minimum accuracy 0.6 mm). Finally, the numerical and experimental data were exported and compared using a custom MatLab 2016b routine (MathWorks Inc., Natick, MA, USA). Furthermore, the force-displacement diagrams, as well as the modes of failure detected by modeling and experimentation, were compared among them, and the maximum stresses calculated in the different model constituents were compared to the mechanical properties of their respective materials.

To provide an example of the model application, the latter was used to evaluate the impact of the implant material stiffness on the stress distribution in the implant.

3. Results

3.1. Kinematics analysis

Fig. 16 compares the displacements of the experimental markers and their numerical representation. To facilitate analysis, the numerical and experimental displacements of the markers are plotted against each other at imposed displacements of the upper part of the construct of 10, 20, 30 and 40 mm. Similar results are observed, indicating that the numerical model represents well the actual kinematics of the limb-prosthesis construct.

3.2. Force-displacement diagrams

Fig. 17 compares the experimentally measured force-displacement diagram and its numerical equivalent. The numerical model exhibits slightly stiffer behavior than the experimental construct, which may be due to model simplifications, such as neglecting the presence of cartilage layers within joints, for example.

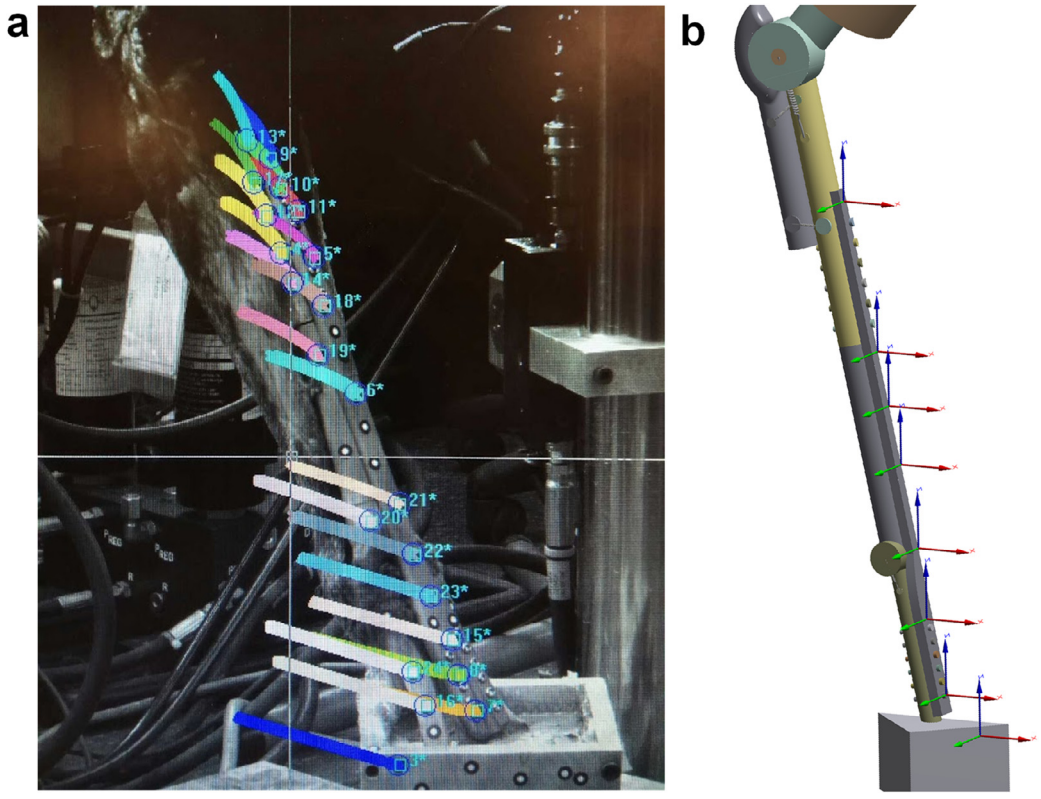

Fig. 15. Markers tracked on the personalized endoprosthesis (a) experimentally and (b) numerically.

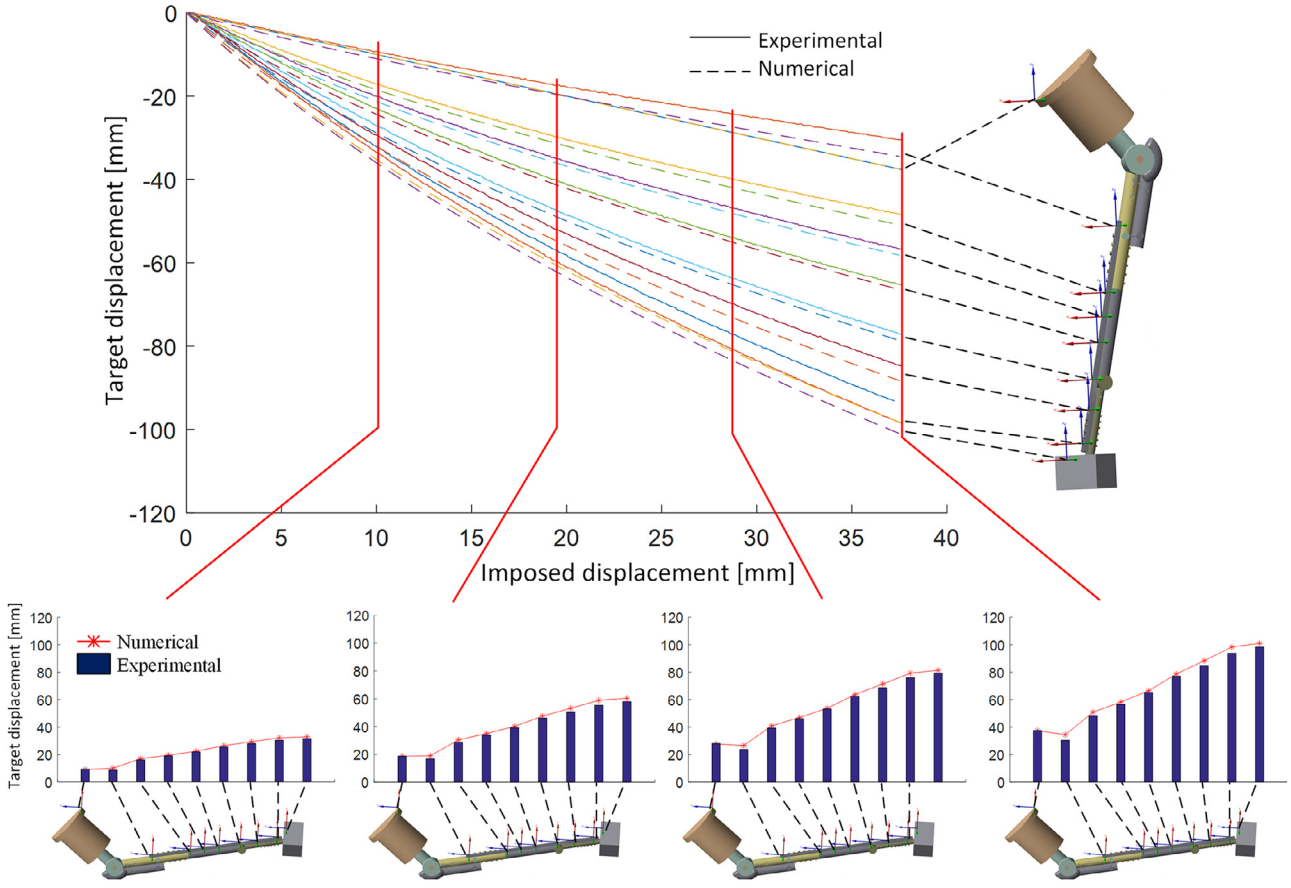

Fig. 16. Displacements of the experimental markers vs numerical probes for imposed displacements of 10, 20, 30 and 40 mm.

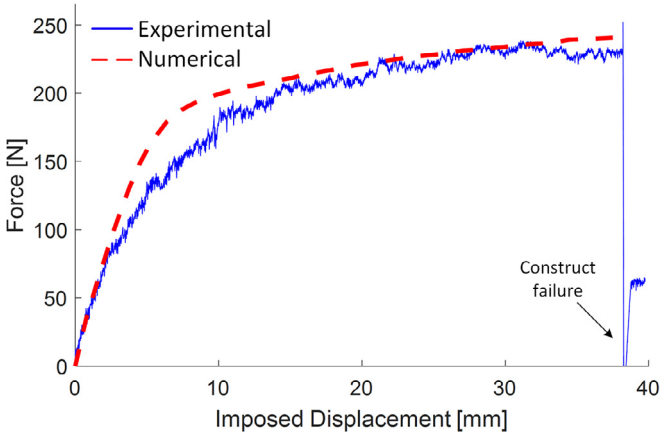

Fig. 17. Force-displacement diagrams obtained by modeling and experimentation.

The limbs suffered failure in the metacarpal region, at a force of 230 N. Failure was due to bending moments generated by the increasing offset between the crosshead axis and the metacarpal embedding zone. The same phenomenon was also observed with the numerical model, with the stress within the metacarpal bone (200 MPa) being higher than the bone ultimate strength reported in the literature (110 MPa) [37].

3.3. Stress analysis of the implant

As an example of the application of the numerical model, a sensitivity analysis was carried out to study the effect of varying implant material stiffness on the stress distribution in the implant. The stress distributions within the endoprosthesis were analyzed numerically and stress risers were identified in the region covering the carpal bones. The maximal calculated stress in the implant was ~300 MPa, which is significantly lower than the yield stress of the additively manufactured Ti64 ($S_y = 945$ MPa, EOS Datasheet). These calculations lead to the conclusion that under this particular loading configuration, the endoprosthesis could resist a threefold increase in load before yielding.

The effect of varying the implant stiffness on the stress distribution in the implant and bone structure can be observed in Fig. 18a. This analysis was realized with the objective of estimating the extent of stress sharing between the implant and the adjacent bones. The stress distribution is improved with a virtual implant material having modulus of elasticity ranging from 25 to 50 GPa. In this case, stress concentration in the implant is reduced, and maximum stresses are evenly distributed over the area between the carpal stress riser and the distal screw fixation. In the metacarpal, bone stress concentration is unaffected, but maximum stresses are however slightly reduced. Currently, the only metallic materials for biomedical applications offering such low moduli of elasticity are superelastic beta-Ti alloys [41]. It is worth noting that by decreasing the implant stiffness, there is a risk of it becoming too compliant, thus increasing stresses in bones and provoking bone failure.

The model can also be used in experiments with various endoprosthesis designs. For example, Fig. 18b shows that transversal pockets can be added in the radial part of the endoprosthesis, allowing a 30% mass reduction, without significantly affecting the maximal stresses in the implant. Additionally, the endoprosthesis design can be modified to reinforce its carpal portion, thus attenuating the stress concentration in this zone and allowing for a better stress distribution.

4. Discussion

4.1. Personalized endoprosthesis

Commercially available prostheses for veterinary limb-sparing surgery are limited in available geometries and sizes. They are only available in two plate lengths and two spacer sizes (VOI, USA), for a total of four configurations. This causes difficulties for veterinary surgeons by requiring them to adapt the plate to the bone geometry and the osteotomy plane, to the available length of the endoprosthesis. The proposed workflow for the design and manufacture of personalized endoprostheses solves these problems by offering prostheses which are perfectly adapted to each patient, and, when combined with the personalized cutting guides, facilitates and reduces the time of surgery.

One of the main advantages of the proposed approach is the versatility of the designs that can be produced by additive manufacturing. For example, if 95% of the radius had to be removed in the patient, the prosthesis design could be modified in order to be reinforced with screws in the ulna, as can be seen in Fig. 19.

The other main problems encountered in limb-sparing surgery are high complication rates due to infection, implant/bone failure and metastasis [6,42]. By using personalized cutting guides and endoprostheses, surgery time could be reduced by 25 to 50%. The time savings come from the non-necessity to bend (contour) the commercially-available plates to better approximate the morphology of bones at the surgery site. The reduction was calculated by dividing the difference in surgery times of the conventional and personalized limb-sparing surgeries by the surgery time of the conventional technique. Surgery duration was calculated from the beginning of the skin incision to the finishing of the closure of the skin incision.

This reduction in surgery duration might reduce the risk of postoperative infection, given that infection risks are linked to surgery time [7,17]. Implant/bone failure risks may also be reduced owing to a more physiological load transfer between endoprostheses and bones via an intimate surface contact between them.

It must be noted that this technological workflow was developed and validated in an academic research environment presenting significant equipment and facility limitations. It may be optimized in a production environment by improving some of the steps, such as bone model reconstruction using programmed algorithms, design of endoprostheses using parametric templates, and automation of finishing post-treatments.

4.2. Modelling and experimental testing

The numerical model of a simplified instrumented limb was validated experimentally both in terms of its kinematics and the construct stiffness, by comparing the marker displacements and the force-displacement diagrams. The numerical and experimental values were in an agreement, despite a slightly stiffer behavior of the model.

The model is a powerful tool that provides indications on the endoprosthesis optimization. It was shown that a better stress distribution in such an implant could be reached if the modulus of elasticity of the implant material was in the 25 to 50 GPa range. This opens up the possibility of replacing a conventional implant material with shape memory alloys, such as beta-Ti alloys, or high strength polymers, such as PEEK or PEKK. These materials are advantageous as they provide better compliance and lower weight, while offering relatively high mechanical resistance. Simultaneously, further optimization of the endoprostheses could be realized by reinforcing areas at-risk and removing material where the implant is not solicited, thus resulting in even more lightweight devices.

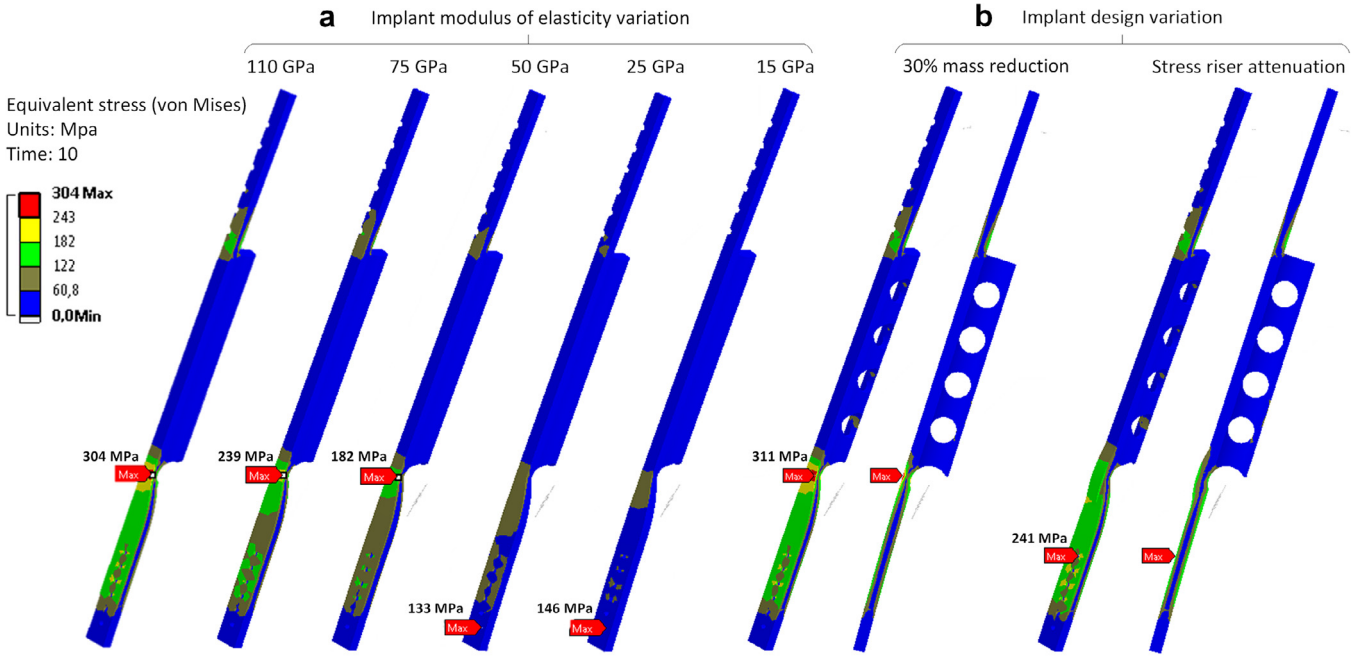

Fig. 18. Stress distribution analysis of the endoprosthesis for (a) endoprosthesis stiffness variation analysis; (b) design variation analysis (Young's modulus of the implant material of 110 GPa).

Fig. 19. (a) Special case of endoprosthesis with bifurcation and (b) 'conventional' personalized endoprosthesis for limb-sparing of the distal radius.

Among the study limitations is that only one experiment was carried out to validate the model. Due to experimental testing limitations, the numerical model was developed with free longitudinal translation of the lower extremity embedding. The fact that the metacarpals were not fixed changed the biomechanics of the constructs as compared to tests performed by Liptak, Ehrhart [14], Horn [27], Pooya, Seguin [28], Shetye [29]. Therefore, a direct comparison of the construct stiffness, load at failure and failure mode obtained in this study with those found in the literature is not appropriate.

However, since the model has been validated for a given set of boundary conditions, the latter could be modified to mimic the published setups and to compare the results obtained with those in the literature. For example, by numerically immobilizing the metacarpal embedding and changing the implant material properties to those of 316 L stainless steel ($E = 200$ GPa, $\nu = 0.33$), the model predicts failures of the construct at a force of 2600 N by fracture of the humerus at the embedded junction. This outcome can be compared with the results of Liptak, Ehrhart [14]: commercial plate-endoprosthesis constructs of the latter study failed at a load varying from 3053±528 to 3445±418 N, depending on the resection or preservation of the ulna, respectively. The failure modes include metacarpus or radius failure (41.7%) and humerus fracture at the potting junction (58.3%). Even though such a comparison involves a high degree of approximation, it constitutes a potentially promising approach.

4.3. Clinical applications

Massive bone defects are replaced with patient-specific 3D-printed implants. Facial, scapular, pelvic, foot, and limb reconstruction using this technology have been reported in humans [43–47]. The more common causes that lead to massive bone defects are tumors and trauma. We have applied the approach described in the current study in the clinical setting in five client-owned dogs affected by osteosarcoma of the distal radius [48]. The turnaround time between data acquisition and shipment of the prosthesis-guide kits varied from 65 to 85 h. The average time distribution

was as follows: ~6 h for reconstruction, ~16.5 h for design, ~20 h for manufacturing, and ~27 h for post-treatments. As earlier stated, in a context of commercial service, some operations could be automated to increase efficiency. The results of the current study will allow optimization of the design of the personal implants in both veterinary and human patients.

5. Conclusion

The objective of this study was twofold: first, to develop a technological workflow for the design and additive manufacturing of personalized endoprostheses and cutting guides and second, to develop and experimentally validate a numerical model of a canine limb instrumented with a personalized endoprosthesis.

A methodology was put in place for the design and manufacturing of personalized endoprostheses in which CT scan data was used to reconstruct the bone models of affected and contralateral limbs. These models served as supports for the design of the personalized endoprosthesis and cutting guide. The designs were validated by the veterinary surgeon and additively manufactured. Following several post-treatments, the prosthesis and cutting guide were ready to be shipped to the clinic where sterilization must be performed before surgery.

A simplified numerical model of an instrumented limb was developed and validated from experimental testing of a cadaveric limb instrumented with a personalized endoprosthesis. The calculated and measured construct kinematics and force-displacement diagrams were in agreement. The validated numerical model can be used to study various effects of input parameters such as material properties, implant geometry and loading conditions, and predicting the implant-limb behavior with a certain degree of confidence.

Several limitations of the model and experimental testing were identified such as the numerical model simplifications, the boundary conditions diverging from biomechanical tests described in the literature and only one experimental validation. The authors recommend further validation of the model using different boundary conditions, as well as testing an endoprosthesis manufactured out of a more flexible material.

Currently, the only benefit of the proposed solution that can be confirmed in canines is a 25 to 50% reduction of surgery duration. Larger clinical studies will determine if complications such as infection and biomechanical failures are decreased.

Competing interests

The authors are inventors on a US Patent #10,342,554 granted on July 9th, 2019 for the cutting guide described in this study.

Funding

This work was supported by the Fonds de développement de l'École de technologie supérieure (FDÉTS) (grant number 909423), the Fonds de recherche du Québec – Nature et technologies (FRQNT) (grant number 205969), V. Brailovski's Discovery grant of the Natural Sciences and Engineering Research Council of Canada (NSERC), the Colorado State University College Research Council, the Aligo Innovation company, the Mitacs Accelerate program (Grant number IT08188), PetCo Foundation, and the Blue Buffalo Foundation Cancer Treatment Support Fund.

Ethical approval

The study involved biomechanical tests on cadaveric dog limbs and a clinical study on five dogs. Approval was received from the Ethics committee of the Montreal Sacred-Heart Hospital Research Center, which is certified by the Canadian Council on Animal Care. In addition, the Clinical Review Board of the Department of Clinical Sciences at the Colorado State University Flint Animal Cancer Center also reviewed and approved the clinical study.

References

[1] Conner BP, Manogharan GP, Martof AN, Rodomsky LM, Rodomsky CM, Jordan DC, et al. Making sense of 3-D printing: creating a map of additive manufacturing products and services. Addit Manuf 2014;1:64–76.
[2] Ventola CL. Medical applications for 3D printing: current and projected uses. Pharm Therap 2014;39:704.
[3] Douglas TS. Additive manufacturing: from implants to organs. SAMJ: S Afr Med J 2014;104:408–9.
[4] Withrow SJ, Page R, Vail DM. Withrow and macewen's small animal clinical oncology - E-book. Elsevier Health Sciences; 2013.
[5] Fan T, Khanna C. Comparative aspects of osteosarcoma pathogenesis in humans and dogs. Vet Sci 2015;2:210–30.
[6] Szewczyk M, Lechowski R, Zabielska K. What do we know about canine osteosarcoma treatment? Review. Vet Res Commun 2015;39:61–7.
[7] Buracco P, Morello E, Martano M, Vasconi ME. Pasteurized tumoral autograft as a novel procedure for limb sparing in the dog: a clinical report. Vet Surg 2002;31:525–32.
[8] Selvarajah GT, Kirpensteijn J. Prognostic and predictive biomarkers of canine osteosarcoma. Vet J 2010;185:28–35.
[9] Spodnick G, Berg J, Rand W, Schelling S, Couto G, Harvey H, et al. Prognosis for dogs with appendicular osteosarcoma treated by amputation alone: 162 cases (1978-1988). J Am Vet Med Assoc 1992;200:995–9.
[10] Bergman PJ, MacEwen EG, Kurzman ID, Henry CJ, Hammer AS, Knapp DW, et al. Amputation and carboplatin for treatment of dogs with osteosarcoma: 48 cases (1991 to 1993). J Vet Intern Med 1996;10:76–81.
[11] Phillips B, Powers BE, Dernell WS, Straw RC, Khanna C, Hogge GS, et al. Use of single-agent carboplatin as adjuvant or neoadjuvant therapy in conjunction with amputation for appendicular osteosarcoma in dogs. J Am Anim Hosp Assoc 2009;45:33–8.
[12] Straw RC, Withrow SJ. Limb-sparing surgery versus amputation for dogs with bone tumors. Vet Clin: Small Animal Pract 1996;26:135–43.
[13] Kuntz TLA CA, Dernell WS, Powers BE, Straw RC, Withrow SJ. Limb salvage surgery for osteosarcoma of the proximal Humerus: outcome in 17 dogs. Vet Surg 1998;27:417–22.
[14] Liptak JM, Ehrhart N, Santoni BG, Wheeler DL. Cortical bone graft and endoprosthesis in the distal radius of Dogs: a biomechanical comparison of two different limb-sparing techniques. Vet Surg 2006b;35:150–60.
[15] Mitchell KE, Boston SE, Kung M, Dry S, Straw RC, Ehrhart NP, et al. Outcomes of limb-sparing surgery using two generations of metal endoprosthesis in 45 dogs with distal radial Osteosarcoma. A veterinary society of surgical oncology retrospective study. Vet Surg: VS 2016;45:36–43.
[16] Withrow S, Thrall D, Straw R, Powers B, Wrigley R, Larue S, et al. Intra-arterial cisplatin with or without radiation in limb-sparing for canine osteosarcoma. Cancer 1993;71:2484–90.
[17] Morello E, Buracco P, Martano M, Peirone B, Capurro C, Valazza A, et al. Bone allografts and adjuvant cisplatin for the treatment of canine appendicular osteosarcoma in 18 dogs. J Small Animal Pract 2001;42:61–6.
[18] Liptak JM, Dernell WS, Lascelles BDX, Larue SM, Jameson VJ, Powers BE, et al. Intraoperative extracorporeal irradiation for limb sparing in 13 dogs. Vet Surg 2004;33:446–56.
[19] Morello E, Vasconi E, Martano M, Peirone B, Buracco P. Pasteurized tumoral autograft and adjuvant chemotherapy for the treatment of canine distal radial osteosarcoma: 13 cases. Vet Surg 2003;32:539–44.
[20] Séguin B, Walsh PJ, Mason DR, Wisner ER, Parmenter JL, Dernell WS. Use of an ipsilateral vascularized ulnar transposition autograft for limb-sparing surgery of the distal radius in dogs: an anatomic and clinical study. Vet Surg 2003;32:69–79.
[21] Uhl JM, Seguin B, Kapatkin AS, Schulz KS, Garcia TC, Stover SM. Mechanical comparison of 3.5 mm broad dynamic compression plate, broad limited-contact dynamic compression plate, and narrow locking compression plate systems using interfragmentary gap models. Vet Surg 2008;37:663–73.
[22] Liptak JM, Dernell WS, Ehrhart N, Lafferty MH, Monteith GJ, Withrow SJ. Cortical allograft and endoprosthesis for limb-sparing surgery in dogs with distal radial Osteosarcoma: a prospective clinical comparison of two different limb-sparing techniques. Vet Surg 2006a;35:518–33.
[23] Wong KC. 3D-printed patient-specific applications in orthopedics. Orthop Res Rev 2016;8:57–66.
[24] Harrysson OLA, Marcellin-Little DJ, Horn TJ. Applications of metal additive manufacturing in veterinary orthopedic surgery. JOM 2015;67:647–54.
[25] Tetsworth K, Block S, Glatt V. Putting 3D modelling and 3D printing into practice: virtual surgery and preoperative planning to reconstruct complex post–traumatic skeletal deformities and defects. SICOT-J 2017;3.
[26] Bray JP, Kersley A, Downing W, Crosse KR, Worth AJ, House AK, et al. Clinical outcomes of patient-specific porous titanium endoprostheses in dogs with tumors of the mandible, radius, or tibia: 12 cases (2013–2016). J Am Vet Med Assoc 2017;251:566–79.
[27] Horn TJ. Development and experimental evaluation of a Novel, patient specific implant for limb sparing surgery. North Carolina State University; 2014.

[28] Pooya HA, Seguin B, Mason DR, Walsh PJ, Taylor KT, Kass PH, et al. Biomechanical comparison of cortical radial graft versus ulnar transposition graft limb-sparing techniques for the distal radial site in dogs. Vet surg: VS 2004;33:301–8.
[29] Shetye S. Development of a novel endoprosthesis for canine limbsparing using a finite element approach. Fort Collins, Colorado: Colorado State University; 2010.
[30] Brailovski V, Petit Y, Lussier B, Seguin B, Brummund M, Timercan A. Limb sparing in mammals using patient-specific endoprostheses and cutting guides. Socovar LP, Universite de Montreal, Colorado State University Research Foundation; 2017.
[31] Haslauer CM, Springer JC, Harrysson OL, Loboa EG, Monteiro-Riviere NA, Marcellin-Little DJ. *In vitro* biocompatibility of titanium alloy discs made using direct metal fabrication. Med Eng Phys 2010;32:645–52.
[32] Murr L, Quinones S, Gaytan S, Lopez M, Rodela A, Martinez E, et al. Microstructure and mechanical behavior of Ti-6Al-4 V produced by rapid-layer manufacturing, for biomedical applications. J Mech Behav Biomed Mater 2009;2:20–32.
[33] Sing SL, An J, Yeong WY, Wiria FE. Laser and electron-beam powder-bed additive manufacturing of metallic implants: a review on processes, materials and designs. J Orthop Res 2016;34:369–85.
[34] Wang X, Xu S, Zhou S, Xu W, Leary M, Choong P, et al. Topological design and additive manufacturing of porous metals for bone scaffolds and orthopaedic implants: a review. Biomaterials 2016;83:127–41.
[35] Yan C, Hao L, Hussein A, Young P. Ti-6Al-4 V triply periodic minimal surface structures for bone implants fabricated via selective laser melting. J Mech Behav Biomed Mater 2015;51:61–73.
[36] Vandenbroucke B, Kruth J-P. Selective laser melting of biocompatible metals for rapid manufacturing of medical parts. Rapid Prototyp J 2007;13:196–203.
[37] Ratner BD, Hoffman AS, Schoen FJ, Lemons JE. Biomaterials Science: an introduction to materials in medicine. Elsevier Science; 2004.
[38] Burstein AH, Currey JD, Frankel VH, Reilly DT. The ultimate properties of bone tissue: the effects of yielding. J Biomech 1972;5:35–42.
[39] Woo S-Y, Gomez M, Akeson W. The time and history-dependent viscoelastic properties of the canine medial collateral ligament. J Biomech Eng 1981;103:293–8.
[40] Sugita T, Amis AA. Anatomic and biomechanical study of the lateral collateral and popliteofibular ligaments. Am J Sports Med 2001;29:466–72.
[41] Sheremetyev V, Brailovski V, Prokoshkin S, Inaekyan K, Dubinskiy S. Functional fatigue behavior of superelastic beta Ti-22Nb-6Zr (at%) alloy for load-bearing biomedical applications. Mater Sci Eng: C 2016;58:935–44.
[42] Morello E, Martano M, Buracco P. Biology, diagnosis and treatment of canine appendicular osteosarcoma: similarities and differences with human osteosarcoma. Vet J 2011;189:268–77.
[43] Park JW, Kang HG, Lim KM, Park DW, Kim JH, Kim HS. Bone tumor resection guide using three-dimensional printing for limb salvage surgery. J Surg Oncol 2018;118:898–905.
[44] Papagelopoulos PJ, Megaloikonomos PD, Korkolopoulou P, Vottis CT, Kontogeorgakos VA, Savvidou OD. Total calcaneus resection and reconstruction using a 3-dimensional printed implant. Orthopedics 2019;42:e282–e2e7.
[45] Beltrami G, Ristori G, Scoccianti G, Tamburini A, Capanna R, Campanacci D, et al. Latissimus dorsi rotational flap combined with a custom-made scapular prosthesis after oncological surgical resection: a report of two patients. BMC Cancer 2018;18:1003.
[46] Chen X, Xu L, Wang Y, Hao Y, Wang L. Image-guided installation of 3D-printed patient-specific implant and its application in pelvic tumor resection and reconstruction surgery. Comput Methods Programs Biomed 2016;125:66–78.
[47] Hsieh T-y, Dedhia R, Cervenka B, Tollefson TT. 3D Printing: current use in facial plastic and reconstructive surgery. Curr Opin Otolaryngol Head Neck Surg 2017;25:291–9.
[48] Séguin B, Pinard C, Lussier B, Williams D, Griffin L, Podell B, et al. Limb-sparing in dogs using patient-specific, 3 dimensional-printed endoprosthesis for distal radial osteosarcoma: a pilot study. Vet Comp Oncol 2019. doi:10.1111/vco.12515.